ACS APPLIED MATERIALS & INTERFACES

Research Article

www.acsami.org

Influence of Noncovalent Modification on Dispersion State of Multiwalled Carbon Nanotubes in Melt-Mixed Immiscible Polymer Blends

Amrita V. Poyekar,[†,‡,§] Arup R. Bhattacharyya,[*,†,‡] Ajay S. Panwar,[†,‡] George P. Simon,[†,§] and D. S. Sutar[∥,⊥]

[†]IITB-Monash Research Academy, Indian Institute of Technology Bombay, Powai, Mumbai 400076, India

[‡]Department of Metallurgical Engineering and Materials Science, Indian Institute of Technology Bombay, Powai, Mumbai 400076, India

[§]Department of Materials Engineering, Monash University, Clayton, Victoria 3800, Australia

[∥]Central Surface Analytical Facility, Indian Institute of Technology Bombay, Mumbai 400076, India

[⊥]Department of Physics, Indian Institute of Technology Bombay, Powai, Mumbai 400076, India

Supporting Information

ABSTRACT: Multiwalled carbon nanotubes (MWNTs) were melt-mixed with polyamide6 (PA6) and acrylonitrile butadiene styrene copolymer (ABS) to obtain electrically conducting composites. MWNTs were noncovalently modified with sodium salt of 6-aminocaproic acid (MWNTs-m1) and 3-pyrenealdehyde (MWNTs-m2) to 'deagglomerate' MWNTs. Raman spectroscopic analysis indicated a G-band shift from ~1581.9 cm^{-1} for pristine MWNTs to ~1590.2 cm^{-1} for MWNTs-m1 and ~1588.8 cm^{-1} for MWNTs-m2, indicating the interaction between MWNTs and the respective modifier molecules. Blends showed 'co-continuous' morphology on the addition of MWNTs. TEM observations showed that a higher population of pristine MWNTs exhibited a 'nanoagglomerated' state in PA6 and ABS phases in the case of a 40/60 PA6/ABS blend, unlike a 60/40 blend, which depicted a higher population of 'individualized' MWNTs. Further, the corresponding blends with MWNTs-m1 and MWNTs-m2 showed 'nanoagglomerated' and 'individualized' MWNTs. Blends with pristine MWNTs showed an increase in DC electrical conductivity with an increase in PA6 concentration in the blend. Moreover, the corresponding blends with MWNTs-m1 and MWNTs-m2 exhibited an increased DC electrical conductivity value as compared to the corresponding blend with pristine MWNTs. Ratio of the intensity (H_1/H_2) of the crystallization peak at lower temperature (H_1) to the intensity of the crystallization peak at higher temperature (H_2) depicted lower values for blends with pristine MWNTs as compared to the corresponding blends with MWNTs-m1 and MWNTs-m2. TGA studies indicated the formation of a thicker 'interphase' involving MWNTs and the interacting polymer chains.

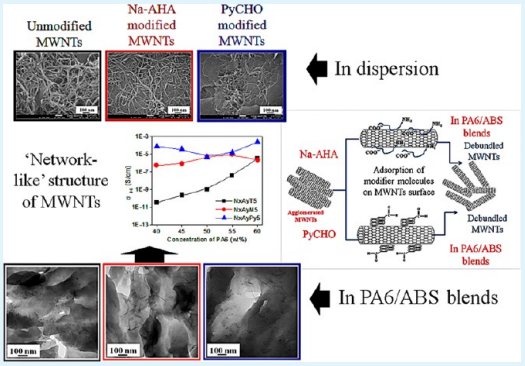

KEYWORDS: *MWNTs, DC electrical conductivity, polymer blends, phase morphology, organic modifiers, interphase*

1. INTRODUCTION

Polymer blends with 'co-continuous' morphology have been exploited as a 'template' to develop electrically conducting composites using multiwalled carbon nanotubes (MWNTs).[1−15] Pristine MWNTs exhibit an entangled and 'agglomerated' state, posing a challenge in dispersing MWNTs in the corresponding blend components, which results in a 'percolated' network at higher MWNTs concentration. The processing parameter optimization during melt-mixing leads to a finer dispersion state of MWNTs in various polymer blends.[1,16−23] In this context, variation in the melt-mixing protocol viz., mixing time, screw rotational speed, and mixing temperature during melt-mixing along with 'sequential' mixing or 'masterbatch' strategy have been exploited to achieve selective distribution of a higher population of MWNTs in a specific phase of 'co-continuous' polymer blends.[8,24−26]

Noncovalent functionalization or modification of the nanotubes is often preferred, which improves the 'dispersibility' of the nanotubes without deteriorating the inherent properties of MWNTs.[27−30] In this context, various studies have reported the modification of MWNTs using a variety of organic molecules such as sodium salt of 6-aminohexanoic acid[31,32] and polyaromatic molecules.[33−35] Encapsulation of MWNTs by various polymers has also been utilized as a strategy to disperse

Received: November 18, 2013
Accepted: June 16, 2014
Published: June 16, 2014

nanotubes homogeneously by utilizing specific interaction between MWNTs and the encapsulating polymer.[36−39] Dispersion of single walled carbon nanotubes (SWNTs) has been facilitated by the conjugated polymer wrapping.[36] A block copolymer of poly(styrene-*b*-pyrene) (PS-*b*-PAH) assists to disperse MWNTs in an epoxy matrix through 'noncovalent' interaction.[37] A 'polymerization-filling technique'[40] has also been reported as an effective way to overcome the filler 'agglomeration,' and as a consequence polymer encapsulated carbon nanotubes have been used as a 'masterbatch.' Styrene maleic anhydride copolymer (SMA) encapsulated SWNTs have exhibited uniform dispersion when melt-mixed with polyamide12 (PA12) through 'reactive coupling' between PA12 and SMA-encapsulated SWNTs.[38]

An exemplary noncovalent organic modifier (sodium salt of 6-amino caproic acid, Na-AHA) has been exploited to induce homogeneous dispersion of MWNTs in a nylon6 (PA6) matrix,[31] PA6/acrylonitrile butadiene styrene copolymer (ABS) blend system,[32,41] PA6/Surlyn blend system,[42] and polypropylene PP/ABS blend system in the presence of PP-*g*-maleic anhydride PP-*g*-MA.[43,44] Na-AHA molecules result in 'deagglomeration' of MWNTs through electrostatic type repulsive forces between the negative charges via the formation of an electrical double layer in aqueous dispersion.[43] Further, a 'melt-interfacial' reaction could be observed between the amine moiety of Na-AHA and the acid end group of PA6 or maleic anhydride functionality of PP-*g*-MA during melt-processing, which induces a 3D 'percolated' structure consisting of 'agglomerate-less' MWNTs. Moreover, phosphonium based various organic modifiers, viz. benzoyl triphenyl phosphonium chloride (BTPC), dodecyl triphenyl phosphonium bromide (DTPB), and octadecyl triphenyl phosphonium bromide (OTPB) encapsulated MWNTs, exhibited a higher DC electrical conductivity in PA6/ABS blends as compared to pristine MWNTs.[45]

Polyaromatic hydrocarbons have been well-reported to interact with the MWNTs surface through '$\pi-\pi$' interaction between the modifier and MWNTs. The molecules with a 'pyrene' moiety interact effectively with the nanotube surface.[33,34,46] The anchoring ability of the pyrene unit on the nanotube surface was exploited to achieve a significant enhancement in the dispersion state of SWNTs in chloroform.[47] Pyrene-capped−polystyrene (PyPS) has been exploited to disperse SWNTs, wherein '$\pi-\pi$' interaction could be envisaged between pyrene and SWNTs. PS/PyPS/SWNTs composites showed significant enhancement in DC electrical conductivity. Amino-pyrene derivative has been used to enhance the dispersion state of MWNTs in a less polar matrix, viz., PP.[48]

In view of this, it has been planned to investigate the influence of noncovalently encapsulated MWNTs to assess the dispersion state of MWNTs via morphological investigation and the electrical conductivity measurement of melt-mixed, 'co-continuous' PA6/ABS blends. The effect of a mixing procedure followed during melt-mixing was investigated on the dispersion state of MWNTs, viz., selective localization in one of the phases, redistribution of MWNTs to another phase, and interface localization, which were assessed via morphological observations. Further, phase morphological alteration in the presence of pristine versus modified MWNTs has also been analyzed to correlate the variation in electrical conductivity in the MWNTs incorporated blends. The use of organic modifiers to improve the dispersion in polymer blends has been extensively reported in the literature. However, the role of processing, various interactions mediated via the use of modifiers, the dispersion of MWNTs in general, localization−redistribution−3D-percolating structure formation of MWNTs in specific, 'interfacial crystallization,' and the 'interphase formation' have not been discussed earlier in understanding the variation of electrical conductivity of the immiscible blends of PA6 and ABS with MWNTs.

2.0. EXPERIMENTAL SECTION

2.1. Materials. Polyamide 6 (PA6; Gujlon M28RC, η_{rel} = 2.8, η_0 = 180 Pa·s at 260 °C) was obtained from GSFC, Gujarat, India. Acrylonitrile−butadiene−styrene copolymer (ABS) (acrylonitrile content of 24 wt %, rubber content of 16.5 wt %, and styrene content of 59.5 wt %) was procured from Bayer India Ltd. Multiwalled carbon nanotubes (MWNTs; grade: NC 3100) were procured from Nanocyl SA, Belgium.[41] 6-Amino caproic acid (M_w = 132.18; purity = 98%, procured from Sigma-Aldrich) was neutralized with a stoichiometric amount of sodium hydroxide (Sisco Research Laboratory, purity = 98%) to prepare sodium salt of 6-amino caproic acid (Na-AHA). 3-Pyrenealdehyde (PyCHO) was obtained from Sigma-Aldrich.

The procedure for making a 1:1 (wt/wt) ratio of MWNTs/Na-AHA (MWNTs-m1) and 1:1 (wt/wt) ratio of MWNTs/PyCHO (MWNTs-m2) can be found in detail elsewhere.[41] Further, MWNTs-m1 and MWNTs-m2 were dried in a vacuum oven at 80 °C for 24 h before melt-mixing.

2.2. Melt-Mixing and Injection Molding. A conical twin-screw microcompounder (MICRO 5, DSM Research, The Netherlands) was utilized for melt-mixing PA6, ABS, and MWNTs. During melt-mixing a simultaneous mixing strategy was used at 260 °C for 15 min of residence time with a screw speed of 100 rpm. Before melt-mixing, PA6 and ABS were vacuum-dried for 24 h at 80 °C. The detailed blend compositions along with the sample codes are mentioned in Table 1.

Table 1. Sample Codes with Their Composition for PA6/ABS Blends with MWNTs

sample	codes
polyamide 6 (PA6)	N
acrylonitrile-butadiene-styrene (ABS)	A
PA6/ABS blends	N_xA_y ($y = 100 - x$)
PA6/ABS blends with 5 wt % unmodified MWNTs 'simultaneous' melt-blending	N_xA_yT5 'x' varies from 40, 45, 50, 55, 60 (wt %)
PA6/ABS blends with 5 wt % Na-AHA modified MWNTs 'simultaneous' melt-blending	N_xA_yM5 'x' varies from 40, 45, 50, 55, 60 (wt %)
PA6/ABS blends with 5 wt % PyCHO modified MWNTs 'simultaneous' melt-blending	N_xA_yPy5 'x' varies from 40, 45, 50, 55, 60 (wt %)

The processing conditions utilized for melt-mixing have been optimized in our earlier study, which are based on the electrical conductivity of the PA6/ABS blends with pristine MWNTs.[49]

In order to make an injection molded specimen, a mini-injection molding machine (DSM Research, Netherlands) was utilized as per ASTM D 638, Type V. The detail injection molding parameters could be found elsewhere.[41]

2.3. Characterization Techniques. *2.3.1. Transmission Electron Microscopic (TEM) Observation.* TEM investigations were carried out on a JEOL JEM-2100 F (Japan) field emission electron microscope with pristine MWNTs, MWNTs-m1, and MWNTs-m2. The sample preparation for the TEM analysis can be found elsewhere.[49]

Leica Ultramicrotome Microsystems (Germany) was used to obtain ultrathin sections of the blend samples with MWNTs at room temperature. Further, the samples were selectively stained with OsO_4 to create the contrast between the phases.

2.3.2. Scanning Electron Microscopic (SEM) Observation. Dispersion state of MWNTs (viz., pristine, MWNTs-m1, MWNTs-m2) was investigated using a FEG-SEM (accelerating voltage = 10 kV,

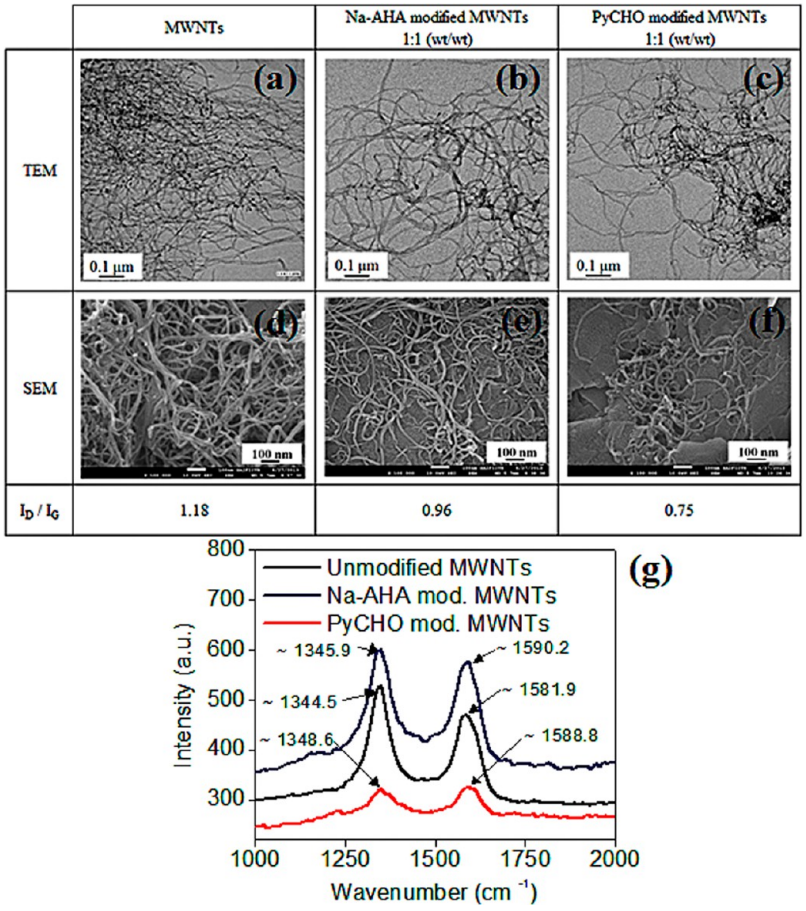

Figure 1. TEM micrographs of (a) unmodified, pristine MWNTs; (b) Na-AHA modified MWNTs; and (c) PyCHO modified MWNTs, 1:1 (wt/wt). SEM micrographs of (d) unmodified, pristine MWNTs; (e) Na-AHA modified MWNTs; and (f) PyCHO modified MWNTs, 1:1 (wt/wt). Characteristic peak intensity ratios (I_D/I_G) for the corresponding MWNTs and (g) Raman spectra for unmodified, pristine MWNTs; Na-AHA modified MWNTs; and PyCHO modified MWNTs (1:1, wt/wt).

JSM-7600F, Japan). The sample preparation for SEM investigation could be found elsewhere.[49]

Further, a Hitachi (S3400N, Japan) instrument was used for extruded samples of the blends with MWNTs. The samples were cryofractured and etched with a selective solvent to remove a specific phase selectively. The sample preparation could be found elsewhere.[49]

2.3.3. Raman Spectroscopic Analysis. A HR 800 micro-Raman (HORIBA Jobin Yovon, France) was utilized to perform Raman spectroscopic analysis for pristine and encapsulated MWNTs samples in the scanning range of 200 to 2000 cm^{-1} with an incident laser excitation wavelength of 514 nm.

2.3.4. FTIR Spectroscopic Analysis. A Nicolet (MAGNA 550, USA) FTIR instrument was used for powdered samples of PA6/ABS blend with pristine MWNTs, MWNTs-m1, and MWNTs-m2. A scanning range of 400−4000 cm^{-1} at room temperature was utilized. A KBr pellet was used for calibration purpose.

2.3.5. X-Ray Photoelectron Spectroscopic (XPS) Analysis. XPS analysis was carried out using the Thermo VG Scientific (MULTILAB, USA). The detail of the instrument could be found in ref 49.

2.3.6. Optical Microscopic Analysis. First, MWNTs dispersion was made in formic acid to dissolve the PA6 phase. The detail of the solution experiment could be found in ref 49. Optical images (Olympus optical microscope, Gx51, USA) were captured for the respective suspensions and were analyzed via software—Olysia m3—to determine the average 'agglomerate' size of MWNTs.

2.3.7. AC Electrical Conductivity Measurements. Novocontrol Technologies (Alpha A analyzer (3 μHz to 20 MHz) and Agilent E4991A RF analyzer (1 MHz - 3 GHz), Germany) were utilized to perform AC electrical conductivity of the respective blends with MWNTs. By fitting Jonscher's 'Universal Power law' equation ($\sigma_{AC} = \sigma_{DC} + A\omega^n$, $0 < n < 1$; 'A' is the constant dependent on temperature, and 'n' is an exponent dependent on the frequency as well as on the temperature), DC electrical conductivity could be obtained from AC conductivity versus frequency plot.

2.3.8. Brunauer-Emmet and Teller Analysis (BET). Surface area analyzer (Smart Instruments, Thane, India) was used to determine specific surface area by nitrogen adsorption method for pristine MWNTs, MWNTs-m1, and MWNTs-m2.

2.3.9. Differential Scanning Calorimetric Analysis. A Q 200 (TA Instruments, USA) modulated differential scanning calorimeter was used to determine the nonisothermal crystallization behavior of PA6 in the respective PA6/ABS blends with MWNTs. The detailed procedure for the protocol of DSC experiment could be found in ref 49.

2.3.10. Thermo Gravimetric Analysis. A Q600 (TA Instruments, USA) simultaneous thermogravimetric analyzer and differential scanning calorimeter (SDT) was utilized to determine the thermal degradation behavior of the blends with MWNTs in a N_2 atmosphere. The detailed procedure regarding TGA analysis could be found in ref 49. The residual weight fraction (%) of MWNTs was determined at 500 °C when both the polymer phases had been completely degraded.

2.3.11. Dispersion Experiment. The dispersion study was carried in the respective solvents of PA6 and ABS for the blends with MWNTs to detect the presence of MWNTs. The detailed procedure could be found in ref 49.

3.0. RESULTS AND DISCUSSION

3.1. Interaction between Organic Modifier Molecules and MWNTs. Surface modification of MWNTs utilizing an organic modifier is a well-established strategy to enhance the

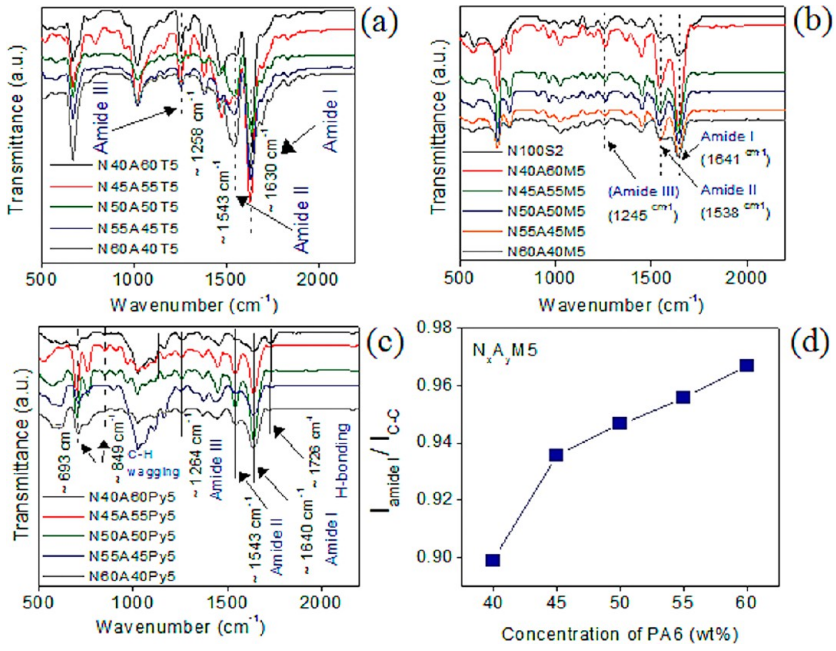

Figure 2. FTIR spectra for PA6/ABS blends of varying blend composition −40/60, 45/55, 50/50, 55/45, and 60/40 (wt/wt) with (a) 5 wt % unmodified MWNTs, (b) 5 wt % Na-AHA modified MWNTs (1:1, wt/wt), and (c) 5 wt % PyCHO modified MWNTs (1:1, wt/wt). (d) Normalized intensity of amide I (at ∼1641 cm^{-1}) peak with respect to the intensity of C−C stretching peak (at ∼1115 cm^{-1}) as a function of PA6 concentration (wt %).

'deagglomeration' of MWNTs. In this context, various types of interactions between the organic modifiers and the MWNTs have been exploited to 'deagglomerate' MWNTs. A detailed comparative assessment of the dispersion state of MWNTs and the interactions existing in the presence of the organic modifier would bring interesting insight in understanding the dispersion state of MWNTs in the immiscible blend of PA6 and ABS.

The morphology of various nanotubes, viz., pristine MWNTs, MWNTs-m1, and MWNTs-m2 as observed from TEM and SEM observations is shown in Figure 1a−c and Figure 1d−f, respectively. Pristine MWNTs exhibit highly 'agglomerated' MWNTs, whereas Na-AHA and PyCHO encapsulated MWNTs depict the presence of less 'agglomerated' MWNTs. The adsorbed organic modifier on the MWNTs surface is evident by the increase in the average diameter of MWNTs as determined from TEM analysis [for pristine MWNTs, D_{avg} ∼ 9.2 nm; for MWNTs-m1, D_{avg} ∼ 13.2 nm; for MWNTs-m2, D_{avg} ∼ 13.5 nm]. Morphological analysis suggests that the modifier molecules are adsorbed on the MWNTs surface and subsequently result in 'deagglomeration' of MWNTs.

Raman spectroscopic analysis exhibits a D-band at ∼1332 cm^{-1} corresponding to the 'double resonance' phenomenon of MWNTs, which involves resonant Raman coupling to the excited photon.[50] Further, a G-band at ∼1582 cm^{-1} is observed due to the ordered graphitic structures corresponding to C═C stretching vibrations in the graphene plane.[50] Raman spectra of pristine and modified MWNTs (Figure 1g) show that the G-band shifts from ∼1581.9 cm^{-1} for pristine MWNTs to ∼1590 cm^{-1} for MWNTs-m1 and ∼1588.8 cm^{-1} for MWNTs-m2. The 'D-band' peak and 'G-band' peak arise as a result of resonant Raman coupling to the phonon excited by the incident photon, which is termed a 'resonance phenomenon.' Variation in the peak position with excitation wavelength could be analyzed on the basis of resonance due to electronic and vibrational densities of state. The vibrational densities of state may vary due to the adsorption of the encapsulated organic modifier on MWNTs, which may alter vibrational modes of MWNTs. A shift to higher wavenumber at a constant laser excitation also indicates fewer intertube interactions, indicating the 'debundling' of nanotubes. A similar shift in G-band for MWNTs has also been earlier noticed in MWNTs-m1 corresponding to 1:1 and 1:4 mixtures of MWNTs and Na-AHA.[31] Moreover, unmodified MWNTs exhibit I_D/I_G value of ∼1.18, whereas MWNTs-m1 show ∼0.96 and MWNTs-m2 depict ∼0.75. Increase in the I_D/I_G ratio is reported to indicate a higher fraction of defects in the graphitic structure.[51] Further, the reduction in the I_D/I_G ratio indicates that MWNTs are well 'deagglomerated' in the presence of the modifier.[43] It has been reported earlier for SWNTs that the corresponding I_D/I_G ratio is decreased after ultrasonication, indicating 'deagglomeration' of SWNTs, due to increased intensity of the tangential mode.[52] This observation may be extended to MWNTs as well, where it is postulated that due to 'deagglomeration' of MWNTs, the photon absorption may increase when a higher ordered graphitic fraction of MWNTs is exposed to the laser. Thus, it may lead to a decrease in I_D/I_G ratio.

The presence of adsorbed Na-AHA on MWNTs is indicated by the shift of the characteristic IR peaks at ∼1413 cm^{-1} and ∼1571 cm^{-1}, which is due to the signature of carboxylate ions (Figure S1a and b in Supporting Information). FTIR spectra of PyCHO and MWNTs-m2 (Figure S2a−d in Supporting Information) showed a shift in vibrational peak of the aromatic ring corresponding to PyCHO molecules from ∼1590 cm^{-1} to ∼1589 cm^{-1}. The carbonyl stretch peak (∼1680 cm^{-1}) corresponding to PyCHO has shown a down-shift of ∼1650 cm^{-1} in the case of MWNTs-m2. Further, the 'wagging' vibration has also shown a down-shift to ∼836 and ∼704 cm^{-1}, respectively. The down-shift of the vibrational peaks manifests

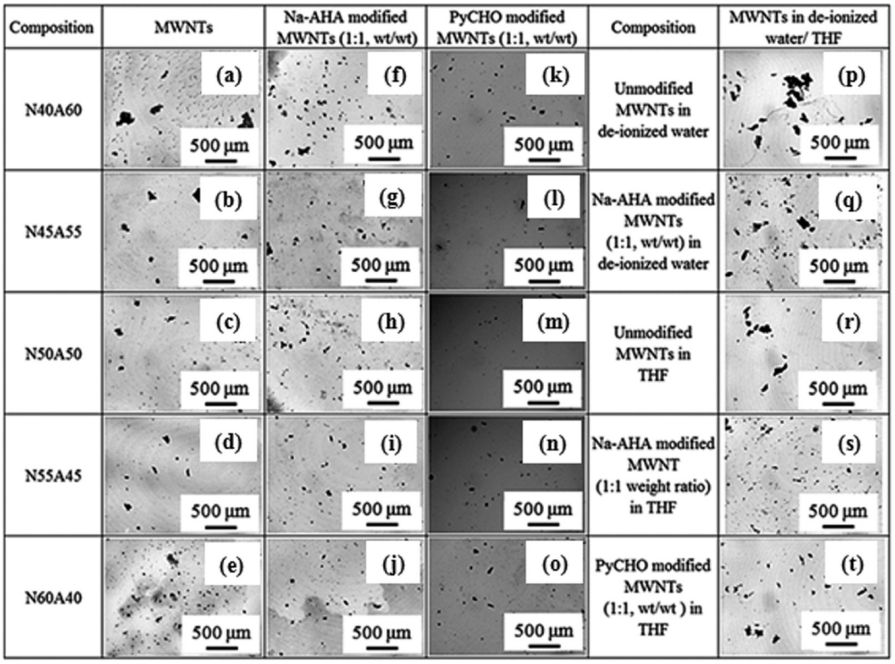

Figure 3. Optical micrographs to determine the remaining MWNTs 'agglomerate' size for PA6/ABS blends with unmodified MWNTs, Na-AHA modified MWNTs, and PyCHO modified MWNTs 1:1 (wt/wt) for varying blend compositions: PA6/ABS blends of varying blend compositions with 5 wt % unmodified MWNTs: 40/60, 45/55, 50/50, 55/45, and 60/40 (wt/wt; a–e), corresponding PA6/ABS blends with 5 wt % Na-AHA modified MWNTs (f–j); blends of respective blend compositions with PyCHO modified MWNTs (1:1 wt/wt; k–o). Optical microscopic images of unmodified MWNTs in deionized water (p) and in THF (r) as well as of Na-AHA modified MWNTs in deionized water (q) and in THF medium (s) and PyCHO modified MWNTs in THF (t) are provided for reference.

'$\pi-\pi$' interaction and 'hydrophobic' interactions between aromatic rings of PyCHO and MWNTs surface.[46]

FTIR spectra of blends with 5 wt % of pristine MWNTs, the corresponding blends with MWNTs-m1, and the corresponding blends with MWNTs-m2 are shown in Figure 2a, b, and c, respectively. In the case of blends with pristine MWNTs (Figure 2a), the FTIR spectra show characteristic signatures of the PA6 phase, which correspond to amide I, amide II, and amide III, respectively. PA6/ABS blends with MWNTs-m1 and PA6/ABS blends with MWNTs-m2 show peaks at ∼1641 cm^{-1}, ∼1538 cm^{-1}, and ∼1245 cm^{-1}, corresponding to amide I, amide II, and amide III peaks (Figure 2b,c). In addition to this observation, additional peaks due to the C–H wagging vibration also could be observed in the FTIR spectra of PA6/ABS blends with MWNTs-m2 at ∼693 cm^{-1} and ∼849 cm^{-1}. Further, a peak at ∼1726 cm^{-1} is observed, which could be due to the H-bonding between –CHO functionality of PyCHO molecules and amine moiety of PA6 chains.[53,54]

Figure 2d depicts the variation in normalized amide peak intensity as a function of PA6 concentration in PA6/ABS blends with MWNTs-m1. The normalized intensity of the amide I peak with respect to the intensity of the peak corresponding to C–C stretching is increased with increasing PA6 concentration. This observation indicates that the extent of 'melt-interfacial' reaction increases with increasing PA6 concentration in the blend compositions. Increasing PA6 concentration in the blend could result in a higher number of –COOH functional groups, which might be available to undergo 'melt-interfacial' reaction with Na-AHA. This would lead to a higher extent of 'melt-interfacial' reaction. Variation in the melt-interfacial reaction may influence the extent of 'preferential' localization of MWNTs-m1 in the PA6 phase of the blends.

BET analysis was carried out to determine the extent of surface coverage of MWNTs due to the adsorption of Na-AHA and PyCHO in the corresponding modified MWNTs. BET theory relates to the rate of adsorption and desorption of one monolayer of adsorbate on the surface.[55] Pristine MWNTs showed a surface area of ∼269.9 m^2/g. MWNTs-m1 and MWNTs-m2 exhibited a surface area of ∼40.7 m^2/g and ∼40.4 m^2/g, respectively. BET analysis also supports the fact that modifier molecules are adsorbed on the MWNTs surface, which in turn results in lower free surface area associated with modified MWNTs.

XPS spectra (Figure S3a and b) show O 1s and C 1s scan for pristine MWNTs and MWNTs-m2. The peaks for carbonyl C and O are observed in the presence of PyCHO molecules in the range of ∼531.65–531.94 eV and ∼286.45–287.92 eV, respectively.[35,56] This observation further substantiates the existence of PyCHO molecules on the MWNTs surface.

3.2. Average Size of MWNTs 'Agglomerates': Influence of Blend Composition and Modification with Organic Modifiers. Average 'agglomerate' size of the remaining MWNTs 'agglomerates' extracted from the PA6 phase was determined using optical microscopic analysis of the blends with pristine MWNTs and corresponding blends with MWNTs-m1 and MWNTs-m2 for different blend compositions (Figure 3a–t). The average 'agglomerate' size of MWNTs for various blend compositions is shown in Table 2. D_{avg} is decreasing monotonically as a function of PA6 concentration for pristine MWNTs (Figure 3a–e; ∼73.7 μm for 40/60 to ∼28.6 μm for 60/40 blend) and MWNTs-m1 (Figure 3f–j; ∼59.9 μm for 40/60 to ∼31.4 μm for 60/40 blend). However, MWNTs-m2 incorporated blends show a progressively increasing D_{avg} as a function of PA6 concentration in the blend (Figure 3k–o; ∼24.3 μm for 40/60 to ∼47.9 μm for 60/

Table 2. Remaining 'Agglomerate' Size of MWNTs in the PA6 Phase in PA6/ABS Blends Determined by the Image Analysis of the Optical Micrographs

wt % of PA6	unmodified MWNTs (D_{avg} in μm)	Na-AHA modified MWNTs (D_{avg} in μm)	PyCHO modified MWNTs (D_{avg} in μm)
40	73.7	59.9	24.3
45	70.5	53.9	27.7
50	64.6	47.4	30.7
55	55.5	44.0	45.1
60	28.6	31.4	48.0

40 blend). Blends with MWNTs-m1 showed lower overall D_{avg} values as compared to blends with pristine MWNTs.

A consistent decrease in D_{avg} in the blends with pristine MWNTs with increasing PA6 concentration may be due to the 'breakup' of large primary MWNTs 'agglomerates' during 'melt-mixing,' facilitated through a higher concentration of PA6 chains, which may wet and infiltrate into the MWNTs 'agglomerates.' Primary 'agglomerate' size is lower in case of blends with MWNTs-m1 (~49 μm in deionized water in Figure 3q, and ~27 μm in THF in Figure 3s) and MWNTs-m2 (~61.2 μm in THF in Figure 3t) irrespective of the dispersion medium as compared to pristine MWNTs (D_{avg} ~108 μm in deionized water as shown in Figure 3p, ~81.5 μm in THF as shown in Figure 3r). 'Melt-interfacial' reaction between PA6 chains and Na-AHA molecules may result in further 'breakup' of MWNTs 'agglomerates' through enhanced infiltration of the PA6 chain into MWNTs 'agglomerates.' Interaction between MWNTs-m2 and the SAN part of the ABS phase would be higher (due to the miscibility between PyCHO and SAN phase) than the interaction between PA6 chain and MWNTs-m2. Therefore, a 40/60 (wt/wt) blend with MWNTs-m2 exhibits a higher population of MWNTs localized in the SAN part of the ABS phase. This observation is also confirmed through the solution experiments shown in Figure S4 provided in the Supporting Information. However, it would be difficult to accommodate MWNTs-m2 in the SAN part of the ABS phase as the PA6 concentration increases in the corresponding blend. Thus, the fraction of MWNTs accumulating in the PA6 phase increases with an increase in PA6 content. This might lead to the higher 'agglomerate' size corresponding to MWNTs in the PA6 phase. The average 'agglomerate' size in the case of MWNTs-m2 is lower as compared to a blend with pristine MWNTs. However, it is higher than the average 'agglomerate' size of the corresponding blends with MWNTs-m1. Hydrogen bonding between PA6 chains and PyCHO molecules was noticed through FTIR analysis. However, this interaction may not be sufficiently strong enough as compared to 'reactive coupling' between PA6 and Na-AHA molecules, which helps PA6 chains not only to effectively interact but also to infiltrate into the primary 'agglomerates' of MWNTs-m1.

The morphology of PA6/ABS neat blends (Figure 4a–e), the corresponding blends with pristine MWNTs (Figure 4f–j), and the respective blends with MWNTs-m1 (Figure 4k–o) and MWNTs-m2 (Figure 4p–t) are depicted in Figure 4a–t. A 40/60 PA6/ABS blend exhibits that PA6 forms the dispersed droplets in the ABS matrix, whereas the blend compositions with lower content of ABS (45/55 and 50/50 PA6/ABS) depict a 'co-continuous' morphology. Further, phase inversion could be observed in 55/45 and 60/40 PA6/ABS blend. On incorporation of pristine MWNTs in the blends, 'co-

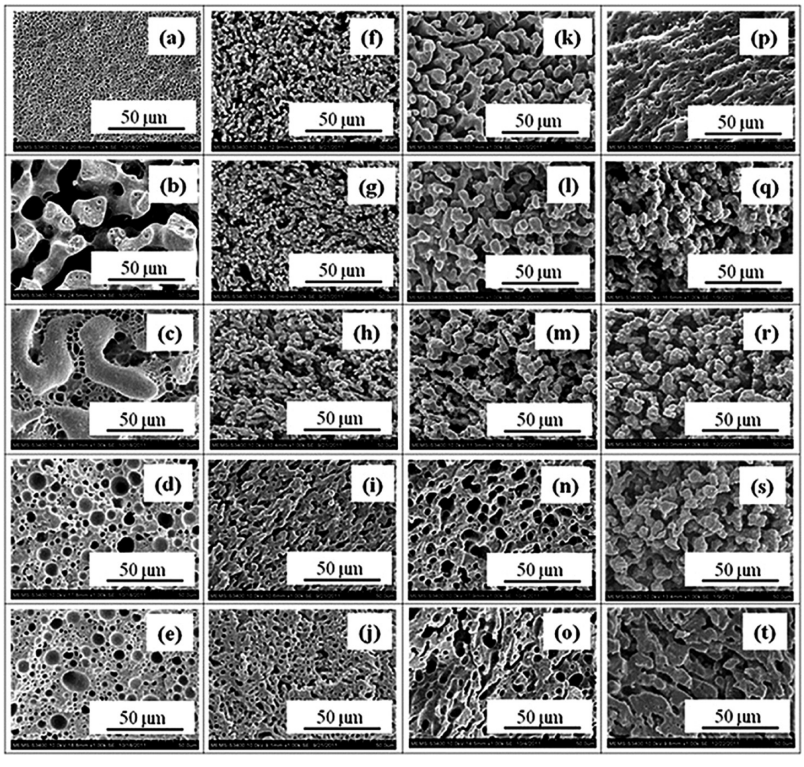

Figure 4. SEM micrographs of neat PA6/ABS blends of varying blend compositions: 40/60, 45/55, 50/50, 55/45, and 60/40 (wt/wt; a–e), corresponding PA6/ABS blends with 5 wt % unmodified MWNTs (f–j); blends of respective blend compositions with Na-AHA modified MWNTs (1:1 wt/wt; k–o) and the respective blend compositions with PyCHO modified MWNTs (1:1 wt/wt) (p–t) where the PA6 phase was removed using formic acid for a and p, and for remaining samples the ABS phase was removed using THF.

continuous' morphology is seen (Figure 4f–j) irrespective of the blend composition. MWNTs-m1 incorporated blends of 40/60, 45/55, and 50/50 (wt/wt) PA6/ABS blend compositions depict a coarse 'co-continuous' phase morphology. With 55/45 and 60/40 blends with MWNTs-m1, the phase morphology changes to a mixed morphology with a 'co-continuous' type and inclusions of elongated ABS droplets. Figure 4p shows a 'matrix-dispersed droplet' type morphology for a 40/60 blend with MWNTs-m2. Further, a well-developed 'co-continuous' morphology is observed for 45/55 to 60/40 blends with MWNTs-m2.

Co-continuous structure formation during melt-mixing of polymer blend depends on the probability of establishment of connectivity between the polymer phases. Therefore, equally viscous polymers melt-mixed in equal volume fractions may result in a 'co-continuous' structure, which corresponds to a 'melt-viscosity' ratio close to 1 and volume fraction of the polymer component of ~0.5. However, often polymers show significantly different 'melt-viscosity' values. In this context, a sufficiently low fraction of low melt-viscosity polymer and high fraction of high melt-viscosity polymer may result in a 'co-continuous' structure as per the qualitative relation reported by Pötschke and Paul.[57] PA6 and ABS exhibit significantly different 'melt-viscosity.' Moreover, MWNTs (surface free energy ~40–45 mN/m[32]) may prefer to localize in the PA6 phase (surface free energy ~36.4 mN/m[32]) rather than ABS (surface free energy ~29.4 mN/m[32]) as the difference in the surface free energy value is lower for PA6. Further, MWNTs localization is also favored by the lower melt-viscosity of the PA6 phase as compared to the highly viscous ABS phase of the corresponding blend. The transformation of the phase morphology may be due to the variation of the viscosity ratio as a higher population of MWNTs selectively localized in the PA6 phase. It is important to note that pristine MWNTs are distributed in both the phases while following a 'simultaneous' mixing strategy, though thermodynamic and kinetic factors suggest the localization of MWNTs preferentially in the PA6 phase.[58]

The variation in the phase morphology of the blends in the presence of MWNTs-m1 may be related to the decrease in melt-viscosity of the PA6 phase due to Na-AHA induced 'chain-scission/plasticization' of PA6.[32] Transformation from a 'co-continuous' structure (50/50 PA6/ABS blend with MWNTs) to a partial 'co-continuous' structure with 'inclusions' of ABS droplets (55/45 and 60/40 blends with MWNTs-m1) indicates that blend composition is near to the 'phase inversion' composition.

The development of 'co-continuous' morphology from the 'matrix-dispersed droplet' morphology may be related to the variation in the melt-viscosity of the 'PA6+MWNTs' phase and 'ABS+MWNTs' phase in the presence of MWNTs-m2. MWNTs localization in the PA6 phase could manifest in an enhanced 'melt-viscosity' of the 'PA6+MWNTs' phase and consequently would lead to the 'co-continuous' type morphology at the end of the 15th minute of melt-mixing. On increasing PA6 concentration, the relative amount of ABS phase decreases in the cases of 45/55, 50/50, 55/45, and 60/40 blends with MWNTs-m2. As mentioned earlier, PyCHO molecules may also engage with PA6 chains through hydrogen bonding, therefore it may result in enhanced melt-viscosity of the 'PA6+MWNTs-m2' phase. Thus, the presence of 'deagglomerated' MWNTs and hydrogen bonding between the PA6 phase and PyCHO molecules may also lead to the change in 'melt-viscosity' ratio, which may develop 'co-continuous' phase morphology.

The percent cocontinuity of PA6 and ABS did not alter significantly in PA6/ABS blends which exhibit 'co-continuous' morphology investigated here. However, it may be interesting to find out the variation in ligament thickness of one of the phases of the blends in the presence of pristine and organically modified MWNTs. The change in ligament size of the PA6 phase as a function of blend composition is shown in Figure 5.

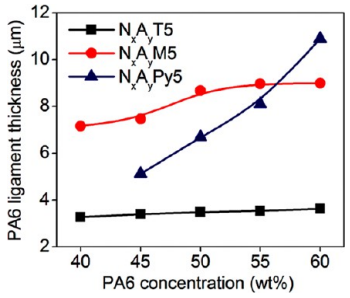

Figure 5. Variation in ligament thickness of PA6 in PA6/ABS blends with unmodified MWNTs (N_xA_yT5), Na-AHA modified MWNTs (1:1, wt/wt; N_xA_yM5), and PyCHO modified MWNTs (1:1, wt/wt; N_xA_yPy5) for varying blend compositions (40/60, 45/55, 50/50, 55/45, and 60/40, wt/wt).

Blends with pristine MWNTs exhibit the lowest ligament size, whereas the corresponding blends with MWNTs-m1 and MWNTs-m2 show a gradual increase in ligament size with increasing PA6 concentration in the corresponding blend. Increased ligament thickness of the PA6 phase may accommodate a higher fraction of MWNTs, which may facilitate the development of 'percolated' structure of MWNTs.

3.3. Localization and Dispersion State of MWNTs in PA6/ABS Blends. PA6/ABS blends with pristine MWNTs display 'co-continuous' morphology for the entire blend composition range. In this connection, the dispersion state of various MWNTs has been analyzed considering two representative blend compositions of PA6/ABS blend, viz., 40/60 and 60/40 compositions.

Higher magnification SEM micrographs (Figure 6a–f) exhibit the dispersion state of pristine and organically encapsulated MWNTs in 40/60 (Figure 6a–c) and 60/40 (Figure 6d–f; wt/wt) PA6/ABS blends. The morphology of the 40/60 PA6/ABS blend with pristine MWNTs (Figure 6a), the corresponding blend with MWNTs-m1 (Figure 6b), and the corresponding blend with MWNTs-m2 (Figure 6c) suggest that it is difficult to differentiate the dispersion state of MWNTs in the corresponding 60/40 blends except MWNTs-m2 based compositions (Figure 6d–f). Figure 6c shows that the 40/60 blend with MWNTs-m2 depicts a higher population of 'agglomerated' MWNTs in the PA6 phase along with 'agglomerated' or 'individualized' MWNTs in the ABS phase. Moreover, the 60/40 blend composition exhibits a 'percolated' structure of MWNTs in both the phases. Therefore, it may be inferred that MWNTs-m2 are localized in both the blend components. SEM observation suggests that it is hard to compare the dispersion state of pristine and organically encapsulated MWNTs in the respective blends of PA6 and ABS.

TEM micrographs of the 40/60 blend with pristine MWNTs, MWNTs-m1, and MWNTs-m2 are depicted in Figure 7a–f.

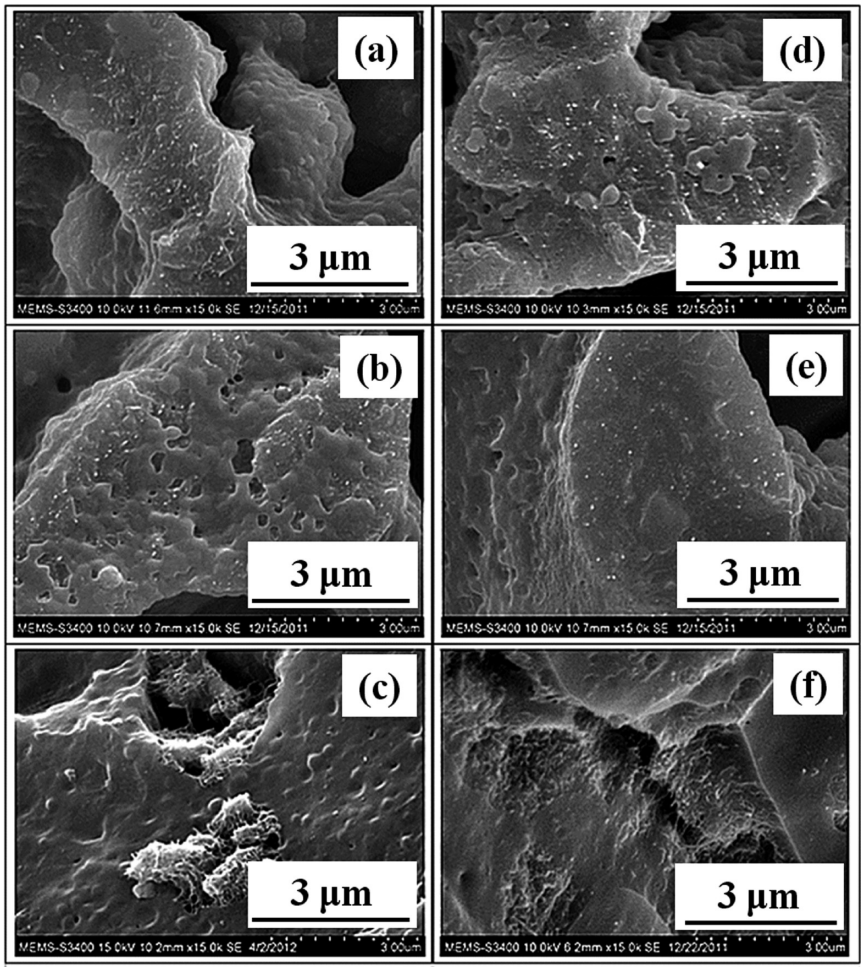

Figure 6. Higher magnification SEM micrographs of 40/60 (wt/wt) PA6/ABS blends with (a) 5 wt % unmodified MWNTs, (b) the corresponding blend composition with 5 wt % Na-AHA modified MWNTs 1:1 (wt/wt; ABS phase has been removed using THF), and (c) the corresponding blend composition with 5 wt % PyCHO modified MWNTs, 1:1 (wt/wt; PA6 phase has been removed by formic acid). High magnification SEM micrographs of 60/40 (wt/wt) PA6/ABS blends with (d) 5 wt % unmodified MWNTs, (e) the corresponding blend composition with 5 wt % Na-AHA modified MWNTs 1:1 (wt/wt), and (f) the corresponding blend composition with 5 wt % PyCHO modified MWNTs, 1:1 (wt/wt; ABS phase has been removed using THF in cases of c, d, and f).

Figure 7a and b show the presence of 'nanoagglomerates' (indicated by outline) of pristine MWNTs in the PA6 and in the SAN phase (of ABS copolymer) of 40/60 blend. Figure 7c and d exhibit 'nanoagglomerates' and 'individually' dispersed MWNTs (indicated by arrows) in the PA6 phase in the corresponding blend with MWNTs-m1 wherein MWNTs could be seen in the ABS phase as well. Further, MWNTs appear perpendicular to the 'interface' between PA6 and ABS phase, where they act like a 'bridge' spanning between the phases.[49] Further, in the case of MWNTs-m2 based composition (Figure 7e and f), MWNTs could be observed at the 'interface' along with their presence in the respective phases.

TEM micrographs of 60/40 blend with pristine MWNTs and the corresponding blends with MWNTs-m1 and MWNTs-m2 are shown in Figure 8a–f. The pristine MWNTs incorporated 60/40 blend (Figure 8a–b) shows a lower fraction of MWNTs 'nanoagglomerates' as compared to 40/60 blend with pristine MWNTs. Pristine MWNTs are mostly 'individualized' forming a 'percolated' structure in the PA6 phase in the case of the 60/40 blend. A fraction of pristine MWNTs is distributed in the ABS phase as well as at the 'interface' (perpendicular to the 'interface' acting like a 'bridge' between the phases). The 60/40 blend with MWNTs-m1 (Figure 8c–d) exhibits a significantly higher population of 'individualized' MWNTs along with the existence of a lower fraction of MWNTs 'nanoagglomerates.' The nanotubes could be observed in the ABS phase and at the interface of the blend. The corresponding blend with MWNTs-m2 could be observed in both PA6 and ABS as well as at the 'interface' of the corresponding blend (Figure 8e–f). Further, a lower population of MWNTs 'nanoagglomerates' is also observed in the case of the 60/40 PA6/ABS blend with MWNTs-m2. In brief, pristine MWNTs could be seen as 'nanoagglomerates' of various sizes in PA6 as well as in the ABS phase. The size of 'nanoagglomerates' of MWNTs decreases in the case of organically encapsulated MWNTs and higher population of 'individualized' MWNTs is observed. Further, a higher population of MWNTs is also observed at the 'interface' of the blend in the case of organically encapsulated MWNTs.

Figure S4 from the Supporting Information depicts the photographic images of MWNTs dispersions in THF solvent, which could assess the localization of MWNTs in the ABS phase. Pristine MWNTs show black coloration associated with MWNTs fraction distributed in the ABS phase. A decreasing trend in the extent of black coloration is observed as a function of increasing PA6 concentration in the blend. MWNTs-m1

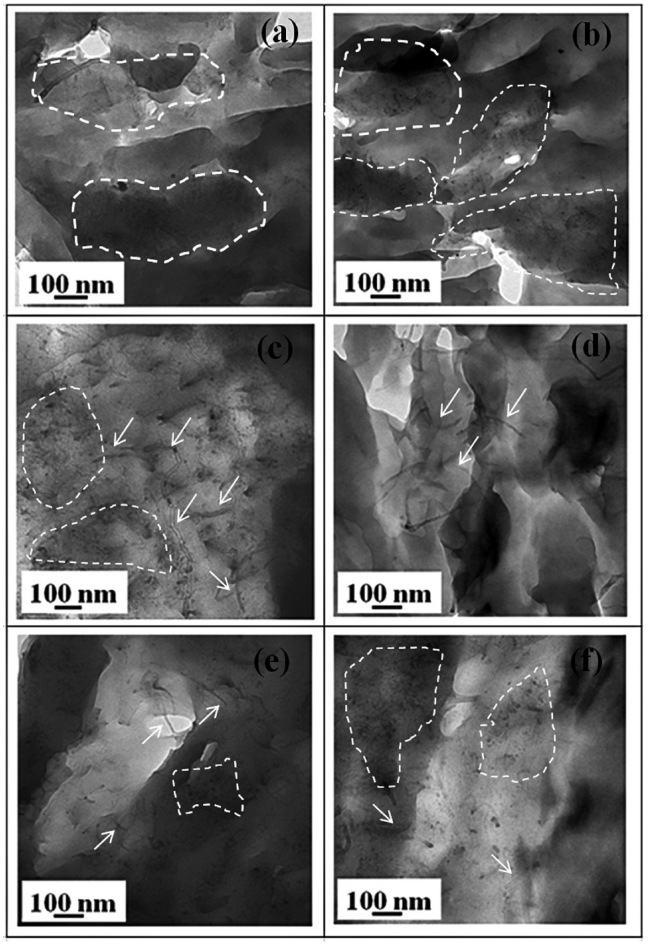

Figure 7. TEM micrographs of the 40/60 (wt/wt) PA6/ABS blend with unmodified MWNTs (a and b), the corresponding blend composition with Na-AHA modified MWNTs 1:1 (wt/wt; c and d), and the corresponding blend composition with PyCHO modified MWNTS 1:1 (wt/wt; e and f), where the ABS phase was stained with OsO_4.

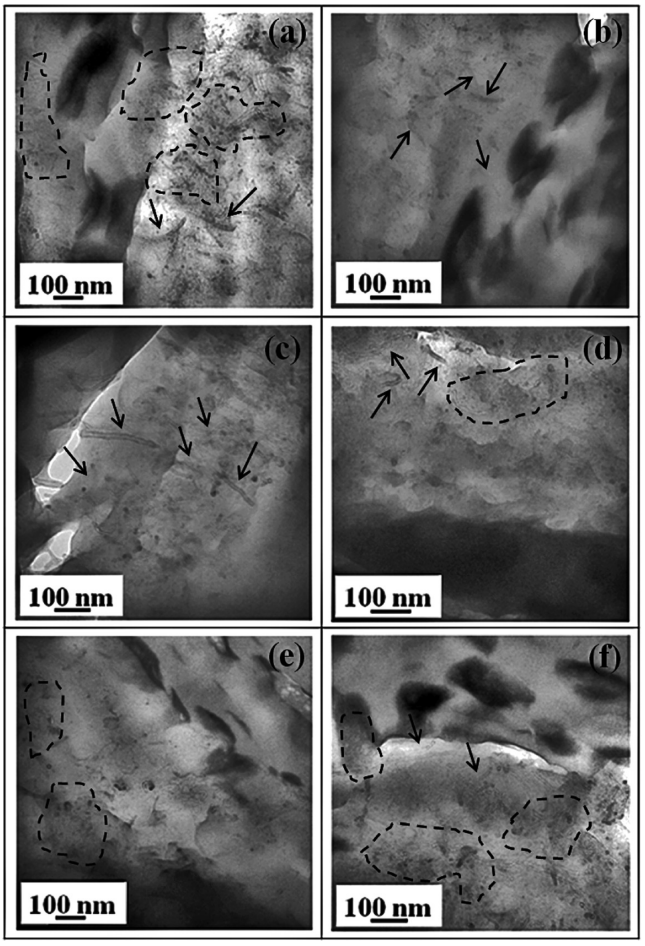

Figure 8. TEM micrographs of the 60/40 (wt/wt) PA6/ABS blend with unmodified MWNTs (a and b), the corresponding blend composition with Na-AHA modified MWNTs 1:1 (wt/wt; c and d), and the corresponding blend composition with PyCHO modified MWNTS 1:1 (wt/wt; e and f), where the ABS phase was stained with OsO_4.

could be seen in the ABS phase for the entire blend composition range of PA6/ABS blend, wherein the extent of black coloration is decreased with increase in PA6 phase concentration in the blend. MWNTs-m2 could be seen in the ABS phase for 40/60 to 50/50 PA6/ABS blends; further, the intensity of black coloration is decreased for 55/45 and 60/40 PA6/ABS blends with MWNTs-m2. Transfer of 'deagglomerated' MWNTs to the ABS phase may be facilitated as compared to pristine MWNTs for MWNTs-m2. Localization of pristine MWNTs and MWNTs-m1 in the ABS phase was earlier reported in PA6/ABS blend prepared via simultaneous melt-mixing.[49]

3.4. Formation of MWNTs 'Network': Influence of the Composition of the Blend and Noncovalent Modifier. Figure 9 depicts the change in DC electrical conductivity of PA6/ABS blends with pristine MWNTs, MWNTs-m1, and MWNTs-m2 as a function of PA6 phase concentration. The DC electrical conductivity increases with an increase in PA6 content of the blend in the case of pristine MWNTs (10^{-11} to 10^{-6} S/cm). Irrespective of blend composition, DC electrical conductivity is also increased in the presence of MWNTs-m1 ($\sim 10^{-7}$ to 10^{-6} S/cm) and MWNTs-m2 ($\sim 10^{-5}$ to 10^{-4} S/cm). The electrical conductivity values with pristine and

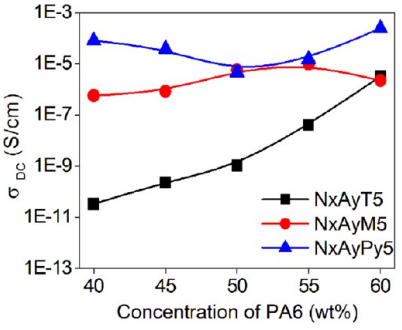

Figure 9. Variation in DC electrical conductivity as a function of PA6 concentration in PA6/ABS blends with 5 wt % unmodified MWNTs, Na-AHA modified MWNTs 1:1 (wt/wt), and PyCHO modified MWNTs 1:1 (wt/wt).

MWNTs-m1 incorporated 60/40 blends are on the order of $\sim 10^{-5}$ S/cm. Our earlier study has shown that the PA6 phase could wet MWNTs effectively at the initial phases of melt-mixing for 60/40 PA6/ABS blend with pristine MWNTs. The infiltration of the PA6 chains in the MWNTs 'agglomerates' at the initial phases of mixing would subsequently lead to the formation of a pristine MWNTs 'network' at a higher PA6

concentration of the blend.[58] Higher electrical conductivity in blends with MWNTs-m1 as compared to pristine MWNTs may be associated with a refined 'percolated' structure of MWNTs. MWNTs-m2 based blends exhibit higher electrical conductivity as compared to MWNTs-m1 based corresponding blends.

As mentioned earlier, a 'simultaneous' melt-mixing protocol drives a fraction of MWNTs in the ABS phase.[49] Redistribution of MWNTs to PA6 phase from the confined ABS phase is suppressed due to high melt-viscosity associated with ABS. The transfer of MWNTs could occur via two steps; initially the contact could be established between the nanotubes and the interface, which was followed by the diffusion of MWNTs to the preferred polymer phase.[59] The 'masterbatch' approach is preferred over a 'simultaneous' mixing protocol to confine nanotubes preferentially in the PA6 phase.[60] However, a minor fraction of MWNTs could be observed in the ABS phase during 'simultaneous' melt-mixing.[49] In presence of Na-AHA (PA6/ABS blend shows DC electrical conductivity of $\sim 8 \times 10^{-10}$ S/cm at 2 wt % MWNTs-m1) and other phosphonium based organic modifiers, viz., BTPC (corresponding DC electrical conductivity of $\sim 10^{-10}$ S/cm), DTPB (corresponding DC electrical conductivity of $\sim 7.1 \times 10^{-7}$ S/cm), and OTPB (corresponding DC electrical conductivity of $\sim 7 \times 10^{-7}$ S/cm), the nanotubes have developed a finer percolated structure of MWNTs.[45] Noncovalent modification of MWNTs by PS-*b*-PAH has shown a finer dispersion state of MWNTs in an epoxy matrix, which was evident by the lower electrical percolation threshold of modified MWNTs (~0.18 wt %) as compared to pristine MWNTs (~0.7 wt %) and enhanced electrical conductivity (corresponding DC electrical conductivity of $\sim 10^{-4}$ S/cm at 1 wt % loading) as compared to the corresponding electrical conductivity of pristine MWNTs (corresponding DC electrical conductivity of $\sim 10^{-6}$ S/cm at 1 wt % loading).[37] This has been explained on the basis of pyrene rings interacting with MWNTs to improve dispersion as well as to facilitate the electron transport. Therefore, it may be commented that the increase in the electrical conductivity in the presence of MWNTs-m2 may be due to a finer 'percolated' structure of MWNTs and 'conjugation' induced enhanced electron transport.

The dispersion state of MWNTs significantly influences the type of 'percolated' structure of MWNTs in the blend. PA6/ABS blends with pristine MWNTs may develop a 'percolated' structure of MWNTs via selective confinement of MWNTs in the PA6 phase. Remaining MWNTs 'agglomerates' observed through optical microscopic analysis could consist of 'nano-agglomerates' of varying sizes based on the blend composition, which is observed through TEM micrographs. Further, the fraction of 'individualized' MWNTs could also be observed through TEM micrographs. Henceforth, it may be commented that 3D 'percolated' structure of MWNTs consists of 'nanoagglomerates' and individualized MWNTs in various PA6/ABS blends with pristine MWNTs. However, PA6/ABS blends with MWNTs-m1 show a significantly refined 'network' of MWNTs, which consists of a higher fraction of 'deagglomerated' MWNTs as well as selective distribution of MWNTs in the PA6 phase. This phenomenon may be supported by a significantly lower value of the remaining MWNTs 'agglomerates' in comparison to the corresponding blends with pristine MWNTs obtained from optical microscopic analysis. The 3D 'network-like' structure of MWNTs-m1 based blends consists predominantly of well separated 'individualized' MWNTs with nanoagglomerates of smaller size. Further, MWNTs-m2 based blends exhibit 3D 'network' formation through 'nanoagglomerates' and 'individualized' MWNTs, which also indicates 'preferential' distribution of MWNTs in the ABS phase.

3.5. Influence of Adsorbed Organic Modifier on MWNTs Surface on the Nonisothermal Crystallization of PA6 Phase. Figure 10a shows the crystallization exotherms

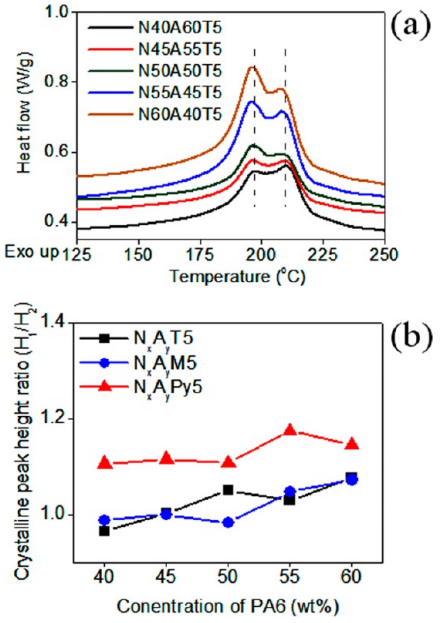

Figure 10. (a) Nonisothermal crystallization exotherms of PA6/ABS blends with 5 wt % unmodified MWNTs for varying blend compositions: 40/60, 45/55, 50/50, 55/45, 60/40. (b) Crystallization peak height ratio of the exothermic peak at a lower temperature to exothermic peak at a higher temperature (H_1/H_2) as a function of PA6 concentration in the blend, indicating the competitive events of heterogeneous nucleated bulk crystallization and 'trans-crystalline' phase formation through 'interfacial crystallization' of the PA6 phase in the presence of MWNTs.

of the PA6 phase of PA6/ABS blends with 5 wt % pristine MWNTs (crystallization exotherms for the corresponding blends with MWNTs-m1 and MWNTs-m2 are provided in Figure S5 of the Supporting Information). It is observed that PA6 exhibits two exothermic peaks in the presence of unmodified MWNTs. The peak observed at higher temperature is due to the 'interfacial crystallization' of the PA6 phase, wherein PA6 chains are directly in contact with the individual MWNTs surface.[61] Further, the peak observed at lower temperatures is associated with the 'heterogeneous nucleation' of the PA6 phase induced by MWNTs. The ratio of the intensity of the crystallization peak at a lower temperature (H_1) to the peak intensity at a higher temperature (H_2) is evaluated in order to investigate the extent of 'interfacial crystallization' of the PA6 phase induced by MWNTs surface (Figure 10b).[61] Higher H_1/H_2 indicates a lower fraction of 'trans-crystalline lamellar' structure, whereas a lower value of H_1/H_2 indicates a higher extent of 'interfacial crystallization.' This is presumably owing to the higher 'available' surface of MWNTs for crystallization of the PA6 phase in addition to the lattice matching between MWNTs and PA6 crystallites. PA6/ABS blends with pristine MWNTs and the corresponding blends with MWNTs-m1 show H_1/H_2 values lower than the values exhibited by PA6/ABS blends with MWNTs-m2. Higher values

of H_1/H_2 suggest the presence of PyCHO molecules on the MWNTs surface, which suppresses the 'interfacial crystallization' of the PA6 phase.

It is to be noted that the finer dispersion state of MWNTs and the enhanced interfacial interaction between PA6 and MWNTs influence the crystallization behavior of PA6 significantly, which exhibit two competitive events, viz., heterogeneous nucleation of PA6 induced by MWNTs and 'trans crystalline lamellar' structure induced 'interfacial crystallization.' It has been established that the Na-AHA molecules are adsorbed on the MWNTs surface during the modification step. However, 'reactive coupling' between the amine moiety of Na-AHA and COOH end groups of PA6 may lead to the removal of Na-AHA molecules from the MWNTs surface. 'Deagglomeration' of MWNTs in the presence of Na-AHA with subsequent removal of Na-AHA from the MWNTs surface may lead to a higher available MWNTs surface area, which subsequently manifests in an enhanced 'interfacial crystallization' of the PA6 phase.

3.6. Formation of 'Interphase' via Interfacial Interaction between Polymer Chain and MWNTs. Figure 11a

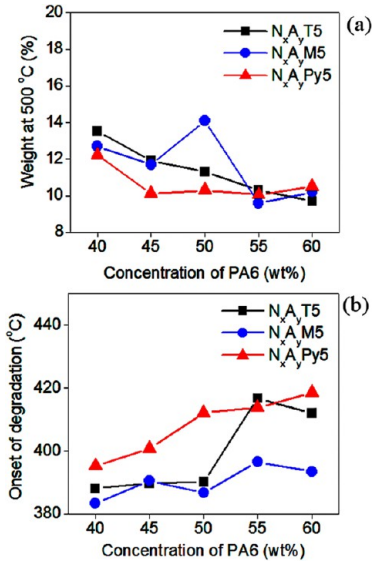

Figure 11. (a) Residual weight at 500 °C as a function of PA6 concentration (wt %) in the blends, indicating the formation of 'interphase' in the presence of various MWNTs. (b) Variation in the 'onset of degradation' with increasing concentration of PA6 (wt %) in the blends.

(the corresponding TGA plots for the blends with MWNTs are shown in Figure S6 of the Supporting Information) shows the change in residual weight fraction of MWNTs at 500 °C for PA6/ABS blends with MWNTs of different concentration of PA6 phase. The experimentally observed residual weight at 500 °C (wherein the complete degradation of both the polymer phases has already occurred in nitrogen atmosphere) is higher than the concentration of MWNTs (5 wt %) present in the respective composites. It is also to be noted that MWNTs are thermally stable up to temperatures much higher than 500 °C in nitrogen atmosphere. PA6/ABS blends with pristine MWNTs and MWNTs-m1 show increased residual weight as compared to the blends with MWNTs-m2.

The excess residual weight is an indication of the formation of the polymer 'interphase,' which is strongly adhered to the MWNTs surface, and thereby the 'interphase' layer could not be degraded even at 500 °C. Pristine MWNTs may allow an effective interaction between the corresponding polymer chains and MWNTs. This may lead to a higher fraction of the 'interphase' layer in the case of PA6/ABS blends with pristine MWNTs, as polymer chains may interact easily with MWNTs in the absence of any modifier molecules. However, polymer phases may be restricted from interacting with the MWNTs surface due to the adsorbed modifier on the MWNTs surface, which may result in a lower fraction of the 'interphase' layer. Interestingly, Na-AHA molecules may be removed from MWNTs surface during the reactive coupling between PA6 and Na-AHA molecules. This phenomenon may result in a higher fraction of 'available' surface for polymer phases to interact, which may lead to the formation of a higher 'interphase' layer. On the contrary, the respective polymer phases may not interact strongly with MWNTs-m2 since PyCHO molecules adhered to the MWNTs surface. Therefore, blends with either pristine or MWNTs-m1 showed higher values of residual weight as compared to the corresponding blends with MWNTs-m2.

During interaction with MWNTs, polymer chains develop a coating or wrapping on the MWNTs surface. During the TGA heating scan, the polymer fraction degrades (between ~300 and ~400 °C) and the mass loss is attributed to polymer adsorbed on the MWNTs surface.[62−64] However, there may be a fraction of the polymer phase strongly adhered to the MWNTs surface that may not degrade even when the bulk polymer phase has been thermally degraded. Therefore, the remaining weight fraction after complete degradation of the polymeric phases could be used to assess polymer/MWNTs interaction.

Morgan et al.[65] found a thermally stable residue/char yield in the case of PMMA/SiO_2 nanocomposites. The residue was attributed to the polymer phase adhered to silica particles, which may exhibit higher thermal stability than the bulk polymer phase that in turn could prevent release of evolved degradation products of the polymeric phase and trapped the polymer phase resulting in a thermally stable residue/char. Further, Baudouin et al.[66] have shown that the polymer fraction strongly adsorbed on the MWNTs surface could not be removed in spite of thorough washing, and this polymer layer has been reported to represent multilayer adsorption owing to entanglements between the chains which are adsorbed on the MWNTs surface and the chains which are not adsorbed.

Figure 11b shows the onset of thermal degradation during a TGA heating scan of the blends with pristine MWNTs and MWNTs-m1 and MWNTs-m2. Blends with MWNTs-m1 showed lower values of onset of degradation temperature as compared to corresponding blends with pristine MWNTs and MWNTs-m2. PA6/ABS blends with MWNTs-m2 show an increase in the onset of thermal degradation temperature. The improved thermal stability in blends with MWNTs-m2 might be due to overall enhanced aromaticity in the structure.

Various interactions between polymer phases, modifier molecules, and MWNTs influence significantly the crystallization behavior of the PA6 phase in the presence of MWNTs, the formation of a thicker 'interphase,' and the electrical conductivity of the blends. Pristine MWNTs exhibit a bare MWNTs surface for polymer interaction, which has resulted in lower H_1/H_2 values and higher residual weight, which indicates a higher extent of 'interphase' formation. However, blends with pristine MWNTs have shown decreased DC electrical

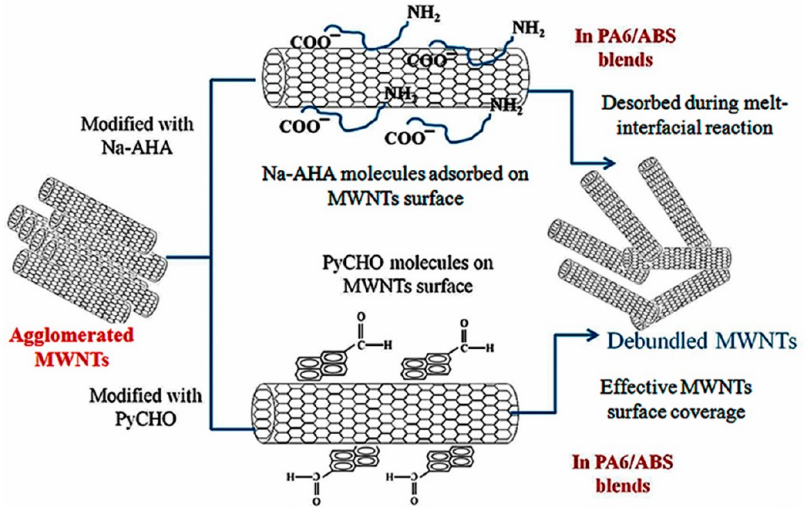

Figure 12. Schematic representation of the possible interactions existing between the organic modifiers and the MWNTs as well as between the modified MWNTs and the blend components PA6 and ABS resulting in the retention of a refined 'network-like' structure of MWNTs.

conductivity due to the highly 'agglomerated' structure of pristine MWNTs, wherein a 60/40 blend shows an exception. A 60/40 blend with pristine MWNTs has shown increased electrical conductivity and has indicated the presence of a higher fraction of 'deagglomerated' MWNTs. It is interesting to observe that blends with MWNTs-m1 have exhibited significantly increased DC electrical conductivity though effective 'interfacial crystallization,' and a higher fraction of 'interphase' formation has been noticed. This observation can be attributed to a finer 'percolated' structure of MWNTs in the presence of Na-AHA via effective 'deagglomeration' of MWNTs as well as 'removal' of Na-AHA molecules from the MWNTs surface due to reactive coupling. It may be commented that the blends with MWNTs-m1 may show higher mechanical properties due to better dispersion of MWNTs and a higher extent of 'interphase' formation. PA6/ABS blends with MWNTs-m2 have shown increased electrical conductivity [the 40/60 blend composition being the exception]. Further, these blends have shown a lower extent of 'interfacial crystallization' and lower fraction of polymer 'interphase' formation as compared to the corresponding blends with MWNTs-m1. However, PA6/ABS blends with MWNTs-m2 have exhibited 10−12 wt % of residual weight, which indicates a higher extent of 'interphase' formation. However, higher DC electrical conductivity values might be achieved through 'deagglomeration' of MWNTs and effective charge transfer via 'conjugation.' It may thus be interpreted that the electrical conductivity of binary 'co-continuous' PA6/ABS blends with pristine and encapsulated MWNTs is significantly influenced by various interactions between polymer phases, modifier molecules, and MWNTs.

The schematic of the probable interactions between the polymer phases with MWNTs and the modifiers when incorporated in the blends is shown in Figure 12. MWNTs exhibit a highly 'agglomerated' state in absence of any surface modification. When the MWNTs are modified with Na-AHA, the Na-AHA molecules are adsorbed on the MWNTs surface and lead to the 'deagglomeration' of MWNTs through charge repulsion between negative charges and via steric factor.[41] However, PyCHO molecules interact effectively with the MWNTs surface through '$\pi-\pi$' interaction. The presence of the PyCHO molecules adsorbed on the MWNTs has led to the effective 'deagglomeration' of MWNTs, probably due to the weakening of forces of attraction.[67] Further, the interaction between the polymer and the encapsulated MWNTs influence the dispersion state and distribution of MWNTs in both the phases. The 'reactive coupling' between PA6 chains and Na-AHA molecules has resulted in a higher 'available' MWNTs surface (which is supported by higher residual weight of the blends with MWNTs and lower H_1/H_2 ratio obtained from the analysis of crystallization behavior of PA6 phase). PyCHO molecules have facilitated the 'deagglomeration' of MWNTs and further facilitated the charge transfer through 'conjugation' (which is supported by higher electrical conductivity values).

CONCLUSION

It may be concluded that the dispersion state and confinement of MWNTs in immiscible, binary blends of PA6 and ABS were influenced by various interactions between the modifier molecules, MWNTs, and respective polymer phases. MWNTs' 'percolated' structure in the blend was influenced by 'selective' distribution of a higher population of MWNTs specifically in one phase of the blend as well as by the formation of 'nanoagglomerated' and 'individualized' MWNTs.

ASSOCIATED CONTENT

Supporting Information

[Figure S1] FTIR spectra for (a) Na-AHA, (b) MWNTs-m1. [Figure S2] FTIR spectra for (a) PyCHO, (b) MWNTs-m2, (c and d) comparison of FTIR spectra of PyCHO and MWNTs-m2 to show the increase in the extent of conjugation in the presence of PyCHO. [Figure S3] XPS spectra for (a) O 1s scan and (b) C 1s scan for pristine MWNTs and MWNTs-m2. [Figure S4] Images of solution experiment wherein THF was used as a solvent for ABS phase of the blends with pristine MWNTs, corresponding blends with MWNTs-m1 and MWNTs-m2 with varying blends composition. [Figure S5] Crystallization exothermic peak of PA6 phase of PA6/ABS blends of varying blend compositions (40/60, 45/55, 50/50, 55/45, and 60/40, wt/wt) with (a) 5 wt % MWNTs-m1 and (b) 5 wt % MWNTs-m2. [Figure S6] TGA plots of PA6/ABS blends of varying blend composition: (a) with 5 wt % pristine MWNTs, (b) with 5 wt % MWNTs-m1, and (c) with 5 wt %

MWNTs-m2. This material is available free of charge via the Internet at http://pubs.acs.org.

AUTHOR INFORMATION

Corresponding Author

*Tel.: +91-22-2576-7634. Fax: +91 22 2572 6975. E-mail: arupranjan@iitb.ac.in.

Funding

Department of Science and Technology (DST), India (Project No. 08DST016)

Notes

The authors declare no competing financial interest.

ACKNOWLEDGMENTS

The authors thank SAIF, CRNTS, 'XPS Central Facility,' and 'Microcompounder Central Facility' at IIT Bombay. One of the authors (A.R.B.) acknowledges Department of Science and Technology (DST), India (Project No. 08DST016) for the financial support.

REFERENCES

(1) Pötschke, P.; Bhattacharyya, A. R.; Janke, A. Morphology and Electrical Resistivity of Melt-Mixed Blends of Polyethylene and Carbon Nanotube Filled Polycarbonate. *Polymer* **2003**, *44*, 8061−8069.

(2) Ramasubramaniam, R.; Chen, J. Homogeneous Carbon Nanotube/Polymer Composites for Electrical Applications. *Appl. Phys. Lett.* **2003**, *83*, 2928−2929.

(3) Pötschke, P.; Bhattacharyya, A. R.; Janke, A. Carbon-Nanotube Filled Polycarbonate Composites Produced by Melt-Mixing and Their Use in Blends with Polyethylene. *Carbon* **2004**, *42*, 965−969.

(4) Meincke, O.; Kaempfer, D.; Weickmann, H.; Friedrich, C.; Vanthauer, M.; Warth, H. Mechanical Properties and Electrical Conductivity of Carbon Nanotube Filled Polyamide-6 and Its Blend with Acrylonitrile-Butadiene-Styrene. *Polymer* **2004**, *45*, 739−748.

(5) Li, Y.; Shimizu, H. Conductive PVDF/PA6/CNTs Nanocomposites Fabricated by Dual Formation of Co-continuous and Nanodispersion Structures. *Macromolecules* **2008**, *41*, 5339−5344.

(6) Khare, R. A.; Bhattacharyya, A. R.; Kulkarni, A. R.; Saroop, M.; Biswas, A. Influence of Multiwall Carbon Nanotubes on Morphology and Electrical Conductivity of PP/ABS Blends. *J. Polym. Sci., Part B: Polym. Phys.* **2008**, *46*, 2286−2295.

(7) Liu, L.; Wang, Y.; Li, Y.; Zhou, Z.; Jiang, C. Improved Fracture Toughness of Immiscible Polypropylene/Ethylene-*co*-Vinyl Acetate Blends with Multiwalled Carbon Nanotubes. *Polymer* **2009**, *50*, 3072−3078.

(8) Göldel, A.; Kasaliwal, G.; Pötschke, P. Selective Localization and Migration of Multiwalled Carbon Nanotubes in Blends of Polycarbonate and Poly(Styrene-Acrylonitrile). *Macromol. Rapid Commun.* **2009**, *30*, 423−429.

(9) Yan, D.; Yang, G. An Innovative Method to Improve the Electrical Conductivity of Multi-Walled Carbon Nanotubes Filled Polyamide 6/Polystyrene Blends. *Mater. Lett.* **2009**, *63*, 1900−1903.

(10) Liu, L.; Wang, Y.; Li, Y.; Wu, J.; Xiang, F.; Zhou, Z. Studies on Fracture Behaviors of Immiscible Polypropylene/Ethylene-*co*-Vinyl Acetate Blends with Multiwalled Carbon Nanotubes. *J. Polym. Sci., Part B: Polym. Phys.* **2009**, *47*, 1331−1344.

(11) Gao, X.; Zhang, S.; Mai, F.; Lin, L.; Deng, Y.; Deng, H.; Fu, Q. Preparation of High Performance Conductive Polymer Fibres from Double Percolated Structure. *J. Mater. Chem.* **2011**, *21*, 6401−6408.

(12) Zonder, L.; Ophir, A.; Kenig, S.; McCarthy, S. The Effect of Carbon Nanotubes on the Rheology and Electrical Resistivity of Polyamide 12/High Density Polyethylene Blends. *Polymer* **2011**, *52*, 5085−5091.

(13) Sun, Y.; Jia, M. Y.; Guo, Z. X.; Yu, J.; Nagai, S. Effect of Styrene-Acrylonitrile on the Electrical Resistivity of Polycarbonate/Multiwalled Carbon Nanotube Composites. *J. Appl. Polym. Sci.* **2011**, *120*, 3224−3232.

(14) Cohen, E.; Zonder, L.; Ophir, A.; Kenig, S.; McCarthy, S.; Barry, C.; Mead, J. Hierarchical Structures Composed of Confined Carbon Nanotubes in Co-continuous Ternary Polymer Blends. *Macromolecules* **2013**, *46*, 1851−1859.

(15) Xiang, F.; Shi, Y.; Li, X.; Huang, T.; Chen, C.; Peng, Y.; Wang, Y. Co-continuous Morphology of Immiscible High Density Polyethylene/Polyamide 6 Blend Induced by Multiwalled Carbon Nanotubes. *Eur. Polym. J.* **2012**, *48*, 350−361.

(16) Andrews, R.; Jacques, D.; Minot, M.; Rantell, T. Fabrication of Carbon Multiwall Nanotube/Polymer Composites by Shear Mixing. *Macromol. Mater. Eng.* **2002**, *287*, 395−403.

(17) Pötschke, P.; Dudkin, S. M.; Alig, I. Dielectric Spectroscopy on Melt-Processed Polycarbonate−Multiwalled Carbon Nanotube Composites. *Polymer* **2003**, *44*, 5023−5030.

(18) Pegel, S.; Pötschke, P.; Petzold, G.; Alig, I.; Dudkin, S. M.; Lellinger, D. Dispersion, Agglomeration, and Network Formation of Multiwalled Carbon Nanotubes in Polycarbonate Melts. *Polymer* **2008**, *49*, 974−984.

(19) Skipa, T.; Lellinger, D.; Saphiannikova, M.; Alig, I. Shear-Stimulated Formation of Multi-Wall Carbon Nanotube Network in Polymer Melts. *Phys. Status Solidi B* **2009**, *246*, 2453−2456.

(20) Krause, B.; Petzold, G.; Pegel, S.; Pötschke, P. Correlation of Carbon Nanotube Dispersibility in Aqueous Surfactant Solutions and Polymers. *Carbon* **2009**, *47*, 602−612.

(21) Krause, B.; Pötschke, P.; Häußler, L. Influence of Small Scale Melt Mixing Conditions on Electrical Resistivity of Carbon Nanotube-Polyamide Composites. *Compos. Sci. Technol.* **2009**, *69*, 1505−1515.

(22) Kasaliwal, G.; Göldel, A.; Pötschke, P. Influence of Processing Conditions in Small-Scale Melt-Mixing and Compression Molding on the Resistivity and Morphology of Polycarbonate-MWNTs Composites. *J. Appl. Polym. Sci.* **2009**, *112*, 3494−3509.

(23) Tambe, P. B.; Bhattacharyya, A. R.; Kulkarni, A. R. The Influence of Melt-Mixing Process Conditions on Electrical Conductivity of Polypropylene/Multiwall Carbon Nanotubes Composites. *J. Appl. Polym. Sci.* **2013**, *127*, 1017−1026.

(24) Göldel, A.; Marmur, A.; Kasaliwal, G. R.; Pötschke, P.; Heinrich, G. Shape-Dependent Localization of Carbon Nanotubes and Carbon Black in an Immiscible Polymer Blend during Melt-Mixing. *Macromolecules* **2011**, *44*, 6094−6102.

(25) Yan, D.; Li, X.; Ma, H. L.; Tang, X. Z.; Zhang, Z.; Yu, Z. Z. Effect of Compounding Sequence on Localization of Carbon Nanotubes and Electrical Properties of Ternary Composites. *Composites, Part A* **2013**, *49*, 35−41.

(26) Fenouillot, F.; Cassagnau, P.; Majesté, J.-C. Uneven Distribution of Nanoparticles in Immiscible Fluids: Morphology Development in Polymer Blends. *Polymer* **2009**, *50*, 1333−1350.

(27) Grady, B. P. *Carbon Nanotubes-Polymer Composites: Manufacture, Properties and Applications*; John Wiley and Sons Inc.: Hoboken, NJ, 2011.

(28) Sahoo, N. G.; Rana, S.; Cho, J. W.; Li, L.; Chan, S. H. Polymer Nanocomposites Based on Functionalized Carbon Nanotubes. *Prog. Polym. Sci.* **2010**, *35*, 837−867.

(29) Roy, N.; Sengupta, R.; Bhowmick, A. K. Modifications of Carbon for Polymer Composites and Nanocomposites. *Prog. Polym. Sci.* **2012**, *37*, 781−819.

(30) Fifield, L. S.; Dalton, L. R.; Addleman, R. S.; Galhotra, R. A.; Engelhard, M. H.; Fryxell, G. E.; Aardahl, C. L. Non-Covalent Functionalization of Carbon Nanotubes with Molecular Anchors Using Supercritical Fluids. *J. Phys. Chem. B* **2004**, *108*, 8737−8741.

(31) Kodgire, P. V.; Bhattacharyya, A. R.; Bose, S.; Gupta, N.; Kulkarni, A. R.; Misra, A. Control of Multiwall Carbon Nanotubes Dispersion in Polyamide6Matrix: An Assessment through Electrical Conductivity. *Chem. Phys. Lett.* **2006**, *432*, 480−485.

(32) Bose, S.; Bhattacharyya, A. R.; Kulkarni, A. R.; Pötschke, P. Electrical, Rheological, and Morphological Studies in Co-Continuous Blends of Polyamide 6 and Acrylonitrile-Butadiene-Styrene with

Multiwall Carbon Nanotubes Prepared by Melt-Blending. *Compos. Sci. Technol.* **2009**, *69*, 365−372.
(33) Tasis, D.; Tagmatarchis, N.; Bianco, A.; Prato, M. Chemistry of Carbon Nanotubes. *Chem. Rev.* **2006**, *106*, 1105−1136.
(34) Simmons, T. J.; Bult, J.; Hashim, D. P.; Linhardt, R. J.; Ajayan, P. M. Non-Covalent Functionalization as an Alternative to Oxidative Acid Treatment of Single Wall Carbon Nanotubes with Applications for Polymer Composites. *ACS Nano* **2009**, *3*, 865−870.
(35) Yang, L. P.; Pan, C. Y. A Non-Covalent Method to Functionalize Multi-Walled Carbon Nanotubes Using Six-Armed Star Poly(L-lactic acid) with a Triphenylene Core. *Macromol. Chem. Phys.* **2008**, *209*, 783−793.
(36) Tuncel, D. Non-Covalent Interactions between Carbon Nanotubes and Conjugated Polymers. *Nanoscale* **2011**, *3*, 3545−3554.
(37) Luan, J.; Zhang, A.; Zheng, Y.; Sun, L. Effect of Pyrene-Modified Multiwalled Carbon Nanotubes on the Properties of Epoxy Composites. *Composites, Part A* **2012**, *43*, 1032−1037.
(38) Bhattacharyya, A. R.; Pötschke, P.; Abdel-Goad, M.; Fischer, D. Effect of Encapsulated SWNT on the Mechanical Properties of Melt Mixed PA12/SWNT composites. *Chem. Phys. Lett.* **2004**, *392*, 28−33.
(39) Kumar, S.; Rath, T.; Mahaling, R. N.; Mukherjee, M.; Khatua, B. B.; Das, C. K. Multi-Walled Carbon Nanotube/ Polymer Composites in the Absence and Presence of Acrylic Elastomer (ACM). *J. Nanosci. Nanotechnol.* **2009**, *9*, 2981−2990.
(40) Bredeau, S.; Peeterbroeck, S.; Bonduel, D.; Alexandre, M.; Dubois, P. From Carbon Nanotube Coatings to High-Performance Polymer Nanocomposites. *Polym. Int.* **2008**, *57*, 547−553.
(41) Bose, S.; Bhattacharyya, A. R.; Kodgire, P. V.; Kulkarni, A. R.; Misra, A. Specific Interactions Induced Dispersion and Confinement of Multi-Walled Carbon Nanotubes in Co-Continuous Polymer Blends. *J. Nanosci. Nanotechnol.* **2008**, *8*, 1867−1879.
(42) Bose, S.; Bhattacharyya, A. R.; Khare, R. A.; Kulkarni, A. R.; Pötschke, P. Specific Interactions and Reactive Coupling Induced Dispersion of Multiwall Carbon Nanotubes in Co-Continuous Polyamide6/Ionomer Blends. *Macromol. Symp.* **2008**, *263*, 11−20.
(43) Khare, R. A.; Bhattacharyya, A. R.; Panwar, A. S.; Bose, S.; Kulkarni, A. R. Dispersion of Multiwall Carbon Nanotubes in Blends of Polypropylene and Acrylonitrile-Butadiene-Styrene. *Polym. Eng. Sci.* **2011**, *51*, 1891−1905.
(44) Khare, R. A.; Bhattacharyya, A. R.; Kulkarni, A. R. Melt-Mixed Polypropylene/Acrylonitrile-Butadiene-Styrene Blends with Multiwall Carbon Nanotubes: Effect of Compatibilizer and Modifier on Morphology and Electrical Conductivity. *J. Appl. Polym. Sci.* **2011**, *120*, 2663−2672.
(45) Bose, S.; Bhattacharyya, A. R.; Khare, R. A.; Kulkarni, A. R.; Patro, T. U.; Sivaraman, P. Tuning the Dispersion of Multiwall Carbon Nanotubes in Co-Continuous Polymer Blends: A Generic Approach. *Nanotechnology* **2008**, *19*, 335704, (8 pp).
(46) Kuang, Y.; Cui, Y.; Zhang, Y.; Yu, Y.; Zhang, X.; Chen, J. A Strategy for the High Dispersion of PtRu Nanoparticles onto Carbon Nanotubes and Their Electrocatalytic Oxidation of Methanol. *Chem.—Eur. J.* **2012**, *18*, 1522−1527.
(47) Yan, Y.; Yang, S.; Cui, J.; Jakisch, L.; Pötschke, P.; Voit, B. Synthesis of Pyrene-Capped Polystyrene for Dispersion of Pristine Single-Walled Carbon Nanotubes. *Polym. Int.* **2011**, *60*, 1425−1433.
(48) Thomassin, J. M.; Huynen, I.; Jerome, R.; Detrembleur, C. Functionalized Polypropylenes as Efficient Dispersing Agents for Carbon Nanotubes in Polypropylene Matrix; Application to Electromagnetic Interference (EMI) Absorber Materials. *Polymer* **2011**, *51*, 115−121.
(49) Poyekar, A. V.; Bhattacharyya, A. R.; Simon, G. P.; Panwar, A. S.; Khare, R. A.; Mishra, J. K.; Dhar, S. Dispersion, Migration, and 'Network-Like' Structure Formation of Multiwall Carbon Nanotubes in Co-Continuous, Binary Immiscible Blends of Polyamide-6 and Acrylonitrile-Butadiene-Styrene Copolymer During Simultaneous Melt-Mixing. *Polym. Eng. Sci.* **2014** (in press), DOI: 10.1002/pen.23904.
(50) Heise, H. M.; Kuckuk, R.; Srivastava, A.; Asthana, B. P. Characterization of Carbon Nanotube Filters and Other Carbonaceous Materials by Raman Spectroscopy−II: Study on Dispersion and Disorder Parameters. *J. Raman Spectrosc.* **2011**, *42*, 294−302.
(51) Athalin, H.; Lefrant, S. A Correlated Method for Quantifying Mixed and Dispersed Carbon Nanotubes: Analysis of the Raman Band Intensities and Evidence of Wavenumber Shift. *J. Raman Spectrosc.* **2005**, *36*, 400−408.
(52) Strano, S. S.; Moore, V. C.; Miller, M. K.; Allen, M. J.; Haroz, E. H.; Kittrell, C.; Hauge, R. H.; Smalley, R. E. The Role of Surfactant Adsorption during Ultrasonication in the Dispersion of Single-Walled Carbon Nanotubes. *J. Nanosci. Nanotechnol.* **2003**, *3*, 81−86.
(53) Pavia, D. L.; Lampman, G. M.; Kriz, G. S. *Introduction to Spectroscopy: A guide for Students of Organic Chemistry*; Saunders Golden Sunburst Series, Harcourt Brace College Publishers: San Diego, CA, 1996.
(54) Guo, L.; Sato, H.; Hashimoto, T.; Ozaki, Y. FTIR Study on Hydrogen-Bonding Interactions in Biodegradable Polymer Blends of Poly(3-hydroxybutyrate) and Poly(4-vinylphenol). *Macromolecules* **2010**, *43*, 3897−3902.
(55) Lehman, J. H.; Terrones, M.; Mansfield, E.; Hurst, K. E.; Meunier, V. Evaluating the Characteristics of Multiwall Carbon Nanotubes. *Carbon* **2011**, *49*, 2581−2602.
(56) Hirashima, Y.; Sato, H.; Suzuki, A. ATR-FTIR Spectroscopic Study on Hydrogen Bonding of Poly(*N*-isopropylacrylamide-*co*-sodium acrylate) Gel. *Macromolecules* **2005**, *38*, 9280−9286.
(57) Pötschke, P.; Paul, D. R. Formation of Co-continuous Structures in Melt-mixed Immiscible Polymer Blends. *J. Macromol. Sci., Part C: Polym. Rev.* **2003**, *C43*, 87−141.
(58) Poyekar, A. V.; Bhattacharyya, A. R.; Simon, G. P.; Panwar, A. S., Evolution of Phase Morphology and 'Network-like' Structure Multi-wall Carbon Nanotubes in Binary Polymer Blends during Melt-Mixing. *Polym. Eng. Sci.* **2014** (in press), DOI: 10.1002/pen.23897.
(59) Göldel, A.; Kasaliwal, G. R.; Pötschke, P.; Heinrich, G. The Kinetics of CNT Transfer between Immiscible Blend Phases during Melt Mixing. *Polymer* **2012**, *53*, 411−421.
(60) Pötschke, P.; Pegel, S.; Claes, M.; Bonduel, D. A Novel Strategy to Incorporate Carbon Nanotubes into Thermoplastic Matrices. *Macromol. Rapid Commun.* **2008**, *29*, 244−251.
(61) Brosse, A. C.; Tencé-Girault, S.; Piccione, P. M.; Leibler, L. Effect of Multi-walled Carbon Nanotubes on the Lamellae Morphology of Polyamide-6. *Polymer* **2008**, *49*, 4680−4686.
(62) Baudouin, A. C.; Bailly, C. Devaux, Interface Localization of Carbon Nanotubes in Blends of Two Copolymers. *J. Polym. Degrad. Stab.* **2010**, *95*, 389−398.
(63) Ciprari, D.; Jacob, K.; Tannenbaum, R. Characterization of Polymer Nanocomposite Interphase and Its Impact on Mechanical Properties. *Macromolecules* **2006**, *39*, 6565−6573.
(64) Verge, P.; Peeterbroeck, S.; Bonnaud, L.; Dubois, P. Investigation on the Dispersion of Carbon Nanotubes in Nitrile Butadiene Rubber: Role of Polymer to Filler Grafting. *Compos. Sci. Technol.* **2010**, *70*, 1453−1459.
(65) Morgan, A. B.; Antonucci, J. M.; VanLandingham, M. R.; Harris, R. H., Jr.; Kashiwagi, T. Thermal and Flammability Properties of a Silica-PMMA Nanocomposite. *Polym. Mater.: Sci. Eng. (1983-2001)* **2000**, *83*, 57−58.
(66) Baudouin, A. C.; Devaux, J.; Bailly, C. Localization of Carbon Nanotubes at the Interface in Blends of Polyamide and Ethylene-Acrylate Copolymer. *Polymer* **2010**, *51*, 1341−1354.
(67) Xue, C. H.; Shi, M.-M.; Yan, Q.-X.; Shao, Z.; Gao, Y.; Wu, G.; Zhang, X.-B.; Yang, Y.; Chen, H.-Z.; Wang, M. Preparation of Water-soluble Multi-walled Carbon Nanotubes by Polymer Dispersant Assisted Exfoliation. *Nanotechnology* **2008**, *19*, 115605.